Full Stokes magnetometry of the active M dwarfs AU Mic and EV Lac with SPIRou

Donati, J.-F.; Cristofari, P.I.; Klein, B.; Finociety, B.; Moutou, C.

A&A, 700, A122 (2025)
https://doi.org/10.1051/0004-6361/202555428

Astronomy & Astrophysics

Full Stokes magnetometry of the active M dwarfs AU Mic and EV Lac with SPIRou

J.-F. Donati[1,⋆], P. I. Cristofari[2], B. Klein[3], B. Finociety[4], and C. Moutou[1]

[1] Univ. de Toulouse, CNRS, IRAP, 14 avenue Belin, 31400 Toulouse, France
[2] Leiden Observatory, Leiden University, Niels Bohrweg 2, 2333 CA Leiden, The Netherlands
[3] Department of Physics, University of Oxford, Oxford OX1 3RH, UK
[4] ACRI-ST, 260 Route du Pin Montard, BP 234, 06904 Sophia-Antipolis, France

Received 7 May 2025 / Accepted 17 June 2025

ABSTRACT

We report in this paper circularly and linearly polarized observations of the young active M dwarfs AU Mic and EV Lac with the near-infrared SPIRou spectropolarimeter at the Canada–France–Hawaii Telescope, collected from August to October 2023 over a few rotation cycles of both stars. Applying Least-Squares Deconvolution (LSD) to our spectra, we detected Zeeman signatures in circular (Stokes V) and linear (Stokes QU) polarization, and Zeeman broadening in unpolarized (Stokes I) LSD profiles, all exhibiting clear rotational modulation. Using the stellar surface tomographic technique of Zeeman-Doppler imaging on our sets of observations, along with a simple parametric description of how the small-scale and large-scale fields relate to each other, we recovered the magnetic topologies of AU Mic and EV Lac successively from LSD Stokes V, Stokes IV and Stokes $IVQU$ profiles, to investigate how the reconstructed maps evolve as we provide more information, and ultimately infer reliable magnetic maps of both stars. We find that AU Mic hosts a fairly simple and mostly poloidal large-scale field aligned with the rotation axis within about 10°, whereas that of EV Lac is more complex, stronger and less axisymmetric. Both stars feature intense small-scale fields, of about 4 kG for AU Mic and 6 kG for EV Lac when averaged over the whole stellar surface. Stokes QU Zeeman signatures allow one to reconstruct stellar magnetic fields more reliably, and are especially useful for stars with more complex fields and low $v \sin i$ like EV Lac.

Key words. techniques: polarimetric – stars: imaging – stars: low-mass – stars: magnetic field – stars: individual: EV Lac – stars: individual: AU Mic

1. Introduction

Magnetic fields play a significant role in the life of low-mass stars, especially during their formation stage, when newly born stars build up from huge molecular clouds of interstellar material and magnetically interact with their circumstellar environment, then throughout their main sequence lifetimes, e.g., when cool stars lose most of their angular momentum through magnetized winds (Donati & Landstreet 2009; Reiners 2012; Kochukhov 2021). These magnetic fields are produced through dynamo processes, i.e., amplified from a small seed field by the interplay of rotation and cyclonic convection operating in stellar convective envelopes for partly convective G, K, and early-M stars, and throughout their interiors for fully convective M dwarfs. The Rossby number, i.e., the ratio of the stellar rotation rate to the convective turnover time, is a key parameter for dynamo processes, with magnetic field strength scaling with the inverse Rossby number until it saturates for stars with Rossby numbers below about 0.1 (e.g., Reiners 2012; Vidotto et al. 2014; See et al. 2015; Reiners et al. 2022).

Magnetic fields of M dwarfs are particularly interesting for studying dynamo processes in low-mass stars other than the Sun, given the wide range of their rotation rates, spanning from under 1 d to over 100 d (e.g., Morin et al. 2010; Donati et al. 2023b), and the wide variety in their internal structures, ranging from partly convective for mature early-M dwarfs to fully convective for late-M or pre-main-sequence (PMS) dwarfs. The recent discovery that very slowly rotating late-M dwarfs can host strong large-scale fields (Lehmann et al. 2024) is quite surprising in this respect. Magnetic field measurements from spectropolarimetric observations have also proven to be particularly efficient in diagnosing rotational modulation of low-mass stars (Hébrard et al. 2016; Fouqué et al. 2023; Donati et al. 2023b), including for the Sun itself (Rescigno et al. 2024). They are also useful for investigating magnetic interactions with potential close-in planets (e.g., Strugarek et al. 2015; Kavanagh et al. 2021), and for studying the impact of large-scale magnetic fields of planet-hosting stars on the habitability of their close-in planets (Vidotto et al. 2013).

Stellar magnetic fields are usually characterized using the Zeeman effect, i.e., the broadening of unpolarized lines and the circular (Stokes V) and linear (Stokes QU) polarization signatures in line profiles that magnetic fields induce in stellar spectra. In low-mass stars other than the Sun, this method was first used to detect small-scale tangled fields from unpolarized (Stokes I) spectra (e.g., Robinson et al. 1980; Saar & Linsky 1985), then large-scale fields through Stokes V spectra (e.g., Donati et al. 1992b, 1997). Tomographic techniques inspired by medical imaging (Skilling & Bryan 1984) were then applied to observations of low-mass stars to infer their large-scale magnetic fields from a time series of rotationally modulated polarized Zeeman signatures (e.g., Donati et al. 1992a, 2006; Morin et al. 2008, 2010; Donati et al. 2023a; Lehmann et al. 2024; Bellotti et al. 2024) and sometimes their small-scale magnetic fields (e.g., Kochukhov et al. 2023). Such studies demonstrate that

⋆ Corresponding author: jean-francois.donati@irap.omp.eu

the dynamos of low-mass stars share similarities with the one operating in the Sun, e.g., with large-scale magnetic topologies exhibiting global polarity switches (e.g., Fares et al. 2009; Boro Saikia et al. 2018; Lehmann et al. 2024), but also significant differences, such as the toroidal component of the magnetic field often being clearly detected at the surface of the star (Donati et al. 1992a; Donati & Landstreet 2009).

Among all magnetic M dwarfs, AU Mic and EV Lac are prototypical examples of key interest for magnetic studies of low-mass stars. With an age of only approximately 20 Myr, AU Mic is a PMS M1 dwarf known to host a debris disk and was recently shown to also harbor a multi-planet system with at least two transiting planets (e.g., Boccaletti et al. 2015; Martioli et al. 2021). Its activity and magnetic field are quite strong, as expected from its young age and relatively short rotation period (Kochukhov & Reiners 2020; Cristofari et al. 2023; Donati et al. 2023a). With an even shorter rotation period, EV Lac is another extremely active M4 dwarf long known for its exceptional rate of energetic flaring and its strong small-scale and apparently atypical large-scale magnetic fields (e.g., Johns-Krull & Valenti 1996; Favata et al. 2000; Reiners & Basri 2007; Morin et al. 2008).

The most recent magnetic analysis of AU Mic showed that modeling the large-scale field from Stokes V data alone can lead to oversimplified magnetic topologies, likely missing not only small-scale structures but potentially large-scale features as well (Donati et al. 2023a). The importance of including Stokes QU Zeeman signatures whenever possible to ensure a more reliable reconstruction of large-scale stellar magnetic topologies was emphasized more than two decades ago in the particular case of chemically peculiar stars (Kochukhov et al. 2004), then for solar-type stars about ten years ago (Rosén et al. 2015), but the relative faintness of these signatures (versus Stokes V ones) renders them difficult to detect and thus to exploit in practice. Observations in the near-infrared (nIR), where the Zeeman effect is stronger, should help greatly in this respect. For these reasons, we initiated a program focusing on AU Mic and EV Lac, based on nIR spectropolarimetric observations recorded in all four Stokes parameters with SPIRou at the Canada-France-Hawaii Telescope (CFHT) atop Maunakea (Donati et al. 2020), to obtain a more precise description of their magnetic topologies.

We review the main properties of AU Mic and EV Lac in Sect. 2 and describe our new spectropolarimetric SPIRou observations in Sect. 3. We then outline our modeling of the magnetic topologies of both stars using the stellar tomographic technique of Zeeman-Doppler imaging (ZDI) in Sect. 4. We summarize our main results and discuss their implications in Sect. 5.

2. The M dwarfs AU Mic and EV Lac

AU Mic (Gl 803) is a $\simeq$20 Myr PMS M1 dwarf known for its prominent debris disk with fast-moving features (Boccaletti et al. 2015, 2018; Gallenne et al. 2022; Lawson et al. 2023), its strong magnetic field (e.g., Kochukhov & Reiners 2020; Klein et al. 2021; Reiners et al. 2022; Cristofari et al. 2023; Donati et al. 2023a, 2025), intense activity level (with starspots, flares and a possible activity cycle, e.g., Ibañez Bustos et al. 2019; Cale et al. 2021; Feinstein et al. 2022; Bloot et al. 2024; Waalkes et al. 2024), and a multiple-planet system featuring at least two transiting Neptune-like planets and two additional candidate planets (Plavchan et al. 2020; Klein et al. 2021; Cale et al. 2021; Martioli et al. 2021; Zicher et al. 2022; Klein et al. 2022; Szabó et al. 2022; Donati et al. 2023a; Wittrock et al. 2023; Mallorquín et al. 2024; Boldog et al. 2025; Yu et al. 2025). With a mass and radius, respectively, equal to $M_\star = 0.60 \pm 0.04$ M$_\odot$ and $R_\star = 0.82 \pm 0.02$ R$_\odot$, AU Mic is still contracting toward the main sequence and has likely started to develop an inner radiative core (Donati et al. 2023a). Seen almost equator-on, AU Mic rotates with a period of $P_{\rm rot} = 4.86$ d, and its spectral lines exhibit significant rotational broadening ($v \sin i = 8.5 \pm 0.2$ km s^{-1}, Donati et al. 2023a).

EV Lac (Gl 873) is an M4 dwarf that has been extensively studied over the past decades for its exceptional flaring properties. It is known to exhibit some of the most energetic flares ever reported for a main-sequence star (Favata et al. 2000; Paudel et al. 2024), making it an ideal laboratory to investigate the extreme magnetic activity of M dwarfs and its potential impact on the habitability of nearby planets, as well as the emergence of life (Feinstein et al. 2022; Paudel et al. 2024). With a rotation period of $P_{\rm rot} = 4.37$ d (e.g., Morin et al. 2008), shorter than that of AU Mic, EV Lac is younger than 1 Gyr (Engle 2024), with a mass and radius respectively equal to $M_\star = 0.32 \pm 0.02$ M$_\odot$ and $R_\star = 0.31 \pm 0.02$ R$_\odot$ (Cristofari et al. 2023). EV Lac hosts a strong small-scale magnetic field of several kG (Johns-Krull & Valenti 1996; Reiners & Basri 2007; Reiners et al. 2022; Cristofari et al. 2023) and an atypical large-scale field with a dipole component reported to be strongly tilted with respect to the stellar rotation axis (Morin et al. 2008; Bellotti et al. 2024). According to evolutionary models (Baraffe et al. 2015; Feiden 2016), EV Lac is located very close to the threshold between partly and fully convective M dwarfs. Depending on its exact mass and radius, it may still be fully convective or have recently started developing a small radiative core. This makes EV Lac and AU Mic structurally similar, despite differences in their masses and radii.

The large- and small-scale magnetic fields of AU Mic and EV Lac have been extensively studied, including through SPIRou observations collected over several seasons (Klein et al. 2021; Cristofari et al. 2023; Donati et al. 2023a; Bellotti et al. 2024; Cristofari et al. 2025; Donati et al. 2025). Both the longitudinal field B_ℓ (i.e., the line-of-sight projected component of the large-scale field averaged over the visible stellar hemisphere, measured from Stokes V line profiles) and the small-scale field B_s (estimated from the broadening of Stokes I line profiles) exhibit rotational modulation. However, these studies relied on either Stokes V and/or Stokes I data, but never included observations in all four Stokes parameters. The magnetic dynamos of AU Mic and EV Lac presumably operate in a saturated regime given their Rossby numbers Ro of 0.14 and 0.058, respectively (Wright et al. 2018). The potential interaction of AU Mic's large-scale magnetic field and its transiting planets has also been investigated in several recent studies (Kavanagh et al. 2021; Alvarado-Gómez et al. 2022; Klein et al. 2022).

The main parameters of both stars are summarized in Table 1.

3. SPIRou observations

We observed AU Mic between 2023 August 02 and September 01, and EV Lac between 2023 September 26 and October 06, with the SPIRou nIR spectropolarimeter (Donati et al. 2020) at CFHT, within a dedicated program (RUNID #23BF08, PI B. Finociety) complemented by additional exposures of AU Mic recorded within the SPICE Large Program (RUNID #23BP45, PI J.-F. Donati). SPIRou collects unpolarized and polarized stellar spectra, covering a wavelength interval of 0.95–2.50 μm at a resolving power of 70 000 in a single exposure. With our main program, we obtained Stokes IQU spectra of

Table 1. Parameters of AU Mic and EV Lac used in this study.

	AU Mic		EV Lac	
distance (pc)	9.714 ± 0.002	Gaia Collaboration (2021)	5.0515 ± 0.0005	Gaia Collaboration (2021)
$T_{\rm eff}$ (K)	3665 ± 31	Cristofari et al. (2023)	3340 ± 31	Cristofari et al. (2023)
$M_\star$ ($M_\odot$)	0.60 ± 0.04	Donati et al. (2023a)	0.32 ± 0.02	Cristofari et al. (2023)
$R_\star$ ($R_\odot$)	0.82 ± 0.02	Donati et al. (2023a)	0.31 ± 0.02	Cristofari et al. (2023)
$P_{\rm rot}$ (d)	4.86	Donati et al. (2023a)	4.37	Morin et al. (2008)
$v \sin i$ (km s^{-1})	8.5 ± 0.2	Donati et al. (2023a)	3.1 ± 0.4	from $P_{\rm rot}$, $R_\star$ and i
i (°)	80	Assumed for ZDI	60	assumed for ZDI
$<B_s>$ (kG)	2.61 ± 0.05	Cristofari et al. (2023)	4.52 ± 0.07	Cristofari et al. (2023)
Rossby number Ro	0.14	Wright et al. (2018)	0.058	Wright et al. (2018)

AU Mic and $IQUV$ observations of EV Lac, while Stokes IV exposures of AU Mic were secured within SPICE as part of our long-term monitoring effort on this key target (Donati et al. 2023a, 2025). Polarization observations with SPIRou usually consist of sequences of four sub-exposures, with each sub-exposure corresponding to a different azimuth of the Fresnel rhomb retarders of the SPIRou polarimetric unit. This procedure was shown to effectively remove systematics in polarization spectra (to first order, see, e.g., Donati et al. 1997). Each recorded sequence yields one Stokes I and one polarized spectrum (either V, Q or U depending on the selected Stokes parameter), as well as one null polarization check (called N) used to diagnose potential instrumental or data reduction issues. We recorded a total of 40 polarization sequences for AU Mic (16 for Stokes V and 12 for each of Stokes Q and U) and 27 exposures for EV Lac (nine for each Stokes V, Q and U parameter), with a complete set of Stokes parameters typically collected on most clear nights. The full log of our observations is provided in Tables A.1 and A.2 in Appendix A.

All SPIRou spectra of AU Mic and EV Lac were processed with `Libre ESpRIT`, the nominal reduction pipeline of ESPaDOnS at CFHT, optimized for spectropolarimetry and adapted for SPIRou (Donati et al. 2020). Subsequently, we applied Least-Squares Deconvolution (LSD, Donati et al. 1997) to the reduced spectra, using a line mask computed from the VALD-3 database (Ryabchikova et al. 2015) for a set of atmospheric parameters roughly matching those of AU Mic and EV Lac ($T_{\rm eff}$ = 3750 K and 3500 K respectively, both with $\log g$ = 5.0). As in previous studies, we only selected atomic lines deeper than 10 percent of the continuum level, for a total of ≃1500 lines, with an average wavelength and Landé factor equal to 1750 nm and 1.2, respectively. Our SPIRou data were also processed with `APERO`, the nominal SPIRou reduction pipeline (Cook et al. 2022), and then analyzed with the line-by-line technique (LBL, Artigau et al. 2022), yielding, for both stars and for each observing night, the differential temperature dT estimated from the variation of spectral lines relative to their median profile (Artigau et al. 2024). We used our dT measurements to infer a relative photometric light curve at SPIRou wavelengths (with temperature changes converted into brightness fluctuations with the Planck function), which was adjusted with ZDI along with the LSD profiles of both stars (see Sect. 4). We obtained light curves at SPIRou wavelengths with full amplitudes of 2.2 and 1.3% for AU Mic and EV Lac, respectively, during our observations, about half the amplitude of those measured with TESS in the I band at other epochs.

To compute the LSD Stokes I and V profiles, we adopted the usual line weights (respectively equal to d and $g\lambda d$, where g, λ, and d denote the Landé factor, wavelength, and relative depth of the line in the mask; see Donati et al. 1997), and the more suitable weight $g^2\lambda^2 d$ to derive LSD Stokes Q and U profiles (following the logic of Donati et al. 1997). The noise levels σ_P in the resulting Stokes LSD profiles ranged from 0.58 to 0.95 for AU Mic (median 0.70, in units of $10^{-4} I_c$, where I_c denotes the continuum intensity); for EV Lac, σ_P ranged from 0.62 to 0.90 (median 0.70) for Stokes Q and U LSD profiles, and from 1.88 to 2.53 (median 2.0) for Stokes V profiles.

Signatures in LSD Stokes V profiles were unsurprisingly detected in both stars, as in previously published SPIRou observations (Donati et al. 2023a; Bellotti et al. 2024). The Zeeman broadening of LSD Stokes I profiles is particularly obvious, as previously discussed in the particular case of AU Mic (Donati et al. 2023a). Clear signatures in LSD Stokes Q and U profiles were unambiguously detected for both stars in most observations (see Sect. 4), confirming the feasibility of full-Stokes magnetometry with SPIRou, at least for strongly magnetic, low-mass stars that are bright enough to yield the requested signal-to-noise ratios (S/Ns). Phases and rotation cycles were derived assuming a rotation period of $P_{\rm rot}$ = 4.86 d and 4.37 d for AU Mic and EV Lac, respectively (see Table 1), counting from an arbitrary starting Barycentric Julian Date (BJD) of 2 459 000 (as in Donati et al. 2023a, for AU Mic).

Finally, we estimated the Zeeman broadening of atomic and molecular lines with ZeeTurbo (as in Cristofari et al. 2023, 2025) using the individual Stokes I spectra of both stars, and derived the corresponding average small-scale magnetic field values over the visible stellar disk $<B_s>$ for each observing night. These values, along with those of dT, are listed in Tables A.1 and A.2.

4. Zeeman-Doppler imaging

Using ZDI, we aimed to reconstruct the magnetic topologies of AU Mic and EV Lac from the sets of rotationally modulated LSD Stokes profiles obtained earlier. Several approaches exist to achieve this, as previously outlined in the particular case of AU Mic (Donati et al. 2023a). The simplest approach is to fit LSD Stokes V profiles only, while ensuring that the average model Stokes I profile is consistent with observations (in both width and equivalent width). This is the classical method used in most ZDI studies, which is best suited to stars with weak to moderate magnetic fields where LSD Stokes I profiles show no clear magnetic broadening (e.g., Lehmann et al. 2024). However, this approach is less appropriate for stars with stronger fields and clear Zeeman broadening in LSD Stokes I profiles (as discussed in Donati et al. 2023a). The second option involves fitting both Stokes I and Stokes V profiles with ZDI, thereby consistently

modeling the Zeeman broadening and circular polarization signatures of line profiles (as achieved for AU Mic in Donati et al. 2023a). In this case, brightness inhomogeneities at the surface of the star can also be reconstructed from LSD Stokes I profiles and photometric data when available. The third and most comprehensive approach is to use all Stokes $IVQU$ data along with photometry to derive the most accurate description of the parent magnetic topology and surface brightness distribution with ZDI. This method is challenging due to the small amplitudes of the Stokes QU Zeeman signatures in most low-mass stars except the strongly magnetic ones, and prior to this work, had been implemented for only one other low-mass star besides the Sun (Rosén et al. 2015).

In the following paragraphs, we describe the results obtained for both AU Mic and EV Lac with these three different approaches using our SPIRou LSD profiles, complemented with light curves derived from dT when fitting LSD Stokes I profiles (for the second and third methods).

4.1. Method description

In practice, ZDI operates as described in previous papers based on SPIRou data. It starts from a small seed magnetic field and a blank brightness distribution, and proceeds iteratively by adding information to the image as it explores the parameter space using conjugate gradient techniques. At each iteration, ZDI compares the synthetic Stokes profiles of the current magnetic image with the observed ones and loops until it reaches the requested level of agreement with the data (i.e., a given reduced chi-square χ^2_r). The surface of the star is typically decomposed into 5000 grid cells, each associated with a value of the local surface brightness relative to that of the quiet photosphere. The magnetic topology is described with a spherical harmonics (SH) expansion using the formalism of Donati et al. (2006) in its revised implementation (Lehmann & Donati 2022; Finociety & Donati 2022), in which the poloidal and toroidal components of the vector field are expressed through three sets of complex SH coefficients: $\alpha_{\ell,m}$ and $\beta_{\ell,m}$ for the poloidal component and $\gamma_{\ell,m}$ for the toroidal component (with ℓ and m denoting the degree and order of the corresponding SH term in the expansion). Given the modest rotational broadening, $v \sin i$, of both stars (see Table 1), we limited the SH expansion that describes the field to $\ell = 10$, i.e., larger than the usual $\ell = 5$ option, to potentially account for the smaller magnetic features that full Stokes magnetometry can reveal (Rosén et al. 2015).

With approximately four spectrally resolved elements (of size $\simeq$4 km s^{-1}) throughout the line profiles for AU Mic and two for EV Lac, there is only $\simeq$160 independent Stokes VQU data points for AU Mic and $\simeq$54 for EV Lac, to reconstruct the 180 SH complex coefficients, i.e., the 360 parameters, describing the large-scale field. This implies that the inversion problem is ill-posed and that regularization is required, especially in the case of EV Lac, even for reconstructions from Stokes $IVQU$ profiles, which are expected to yield a unique solution under ideal conditions (Piskunov 2005). ZDI selects the simplest solution among the multiple possibilities, i.e., the one with minimum information or maximum entropy, that matches the data at the requested χ^2_r level, following the approach of Skilling & Bryan (1984).

To compute local synthetic Stokes $IVQU$ profiles from each grid cell, we again used the Unno-Rachkovsky analytical solution to the polarized radiative transfer equation in a plane-parallel Milne-Eddington atmosphere (Landi degl'Innocenti & Landolfi 2004). We then integrated the spectral contributions from all visible grid cells, assuming a linear center-to-limb darkening law for the continuum, with a coefficient of 0.3, to obtain the global synthetic profiles at each observed rotation phase. The mean wavelength and Landé factor of our synthetic profiles are mirrored from those of our LSD profiles, i.e., 1700 nm and 1.2. When focusing on LSD Stokes V profiles alone, we assumed a Doppler width v_D of the local profile equal to $v_D = 5.3$ km s^{-1} (as in Donati et al. 2023a) so that synthetic Stokes I profiles were as wide as the observed ones given the assumed $v \sin i$ (see Table 1) and minimal Zeeman broadening. When simultaneously fitting LSD Stokes IV or Stokes $IVQU$ profiles, we assumed a more realistic Doppler width of $v_D = 3.5$ km s^{-1}, yielding a profile width that matched the asymptotic width of LSD profiles from atomic lines with decreasing Landé factors (see Donati et al. 2023a).

We also introduced the polarization filling factor f_P (assumed constant over the whole star) which describes the fraction of each grid cell contributing to the large-scale field and to the Stokes V, Q and U profiles. This implies a magnetic field of B_P/f_P within the magnetic portion of a cell and a magnetic flux of B_P over the whole cell. Similarly, we assumed that a fraction f_I of each grid cell (the filling factor of the small-scale field, again equal for all cells) hosts small-scale fields of strength B_P/f_P, implying a small-scale magnetic flux over the whole cell equal to $B_I = B_P f_I/f_P$. This simple parametric approach within ZDI was used to empirically reproduce the coexistence of small- and large-scale fields at the surface of M dwarfs, as inferred from both observations and simulations (e.g., Kochukhov 2021; Yadav et al. 2015). To compute the synthetic light curve, we summed the photometric contributions estimated from the local brightness and limb angle of all visible cells at each observed rotation phase. Finally, we assumed that the projection of the stellar rotation axis on the plane of the sky makes an angle ψ with respect to the reference direction of the polarimeter (i.e., east-west), measured anticlockwise. The values of i and $v \sin i$ for AU Mic and EV Lac were adopted from previous studies (see Table 1). None of the parameters describing the local line profile, particularly v_D, f_P and f_I, were assumed to depend on the magnetic field.

One challenge of the third approach was to realistically model the observed LSD Stokes $IQUV$ profiles, which are essentially weighted averages of about 1500 real spectral lines with different strengths, Zeeman sensitivities and patterns, using a single virtual line described as a simple Zeeman triplet. Whereas this approach is relatively straightforward for stars with weak magnetic fields, its implementation is more challenging for strongly magnetic stars such as AU Mic and EV Lac. It required careful adjustment of line parameters, particularly v_D, f_P and f_I, for the model to match observations. This method has already been shown to be successful at simultaneously reproducing sets of observed LSD Stokes IV profiles in the case of AU Mic (Donati et al. 2023a), and it suggested that the inferred large-scale field is significantly underestimated in strongly magnetic stars when focusing on Stokes V profiles alone (as in, e.g., Klein et al. 2021; Bellotti et al. 2024). Generalizing this approach to the simultaneous modeling of LSD Stokes $IVQU$ profiles makes parameter tuning even more essential. Nonetheless, we succeeded in achieving a reasonably good fit to full Stokes spectropolarimetric observations of both AU Mic and EV Lac, as described in the following paragraphs. The alternative approach described in Rosén et al. (2015), based on constructing tables of synthetic LSD profiles for a wide variety of field strengths and orientations from synthetic polarized spectra, is difficult to apply at nIR wavelengths where synthetic spectra computed from various sets of atmospheric models differ significantly (e.g.,

Cristofari et al. 2022). Moreover, these models do not provide a reliable description of the spectral content of high-resolution observations of M dwarfs (Artigau et al. 2018, 2024) except in narrow regions where line parameters were manually adjusted (e.g., Cristofari et al. 2023).

When fitting LSD Stokes $IVQU$ profiles, we used only the Stokes I profiles associated with the Stokes V data, excluding the (mostly redundant) Stokes I profiles associated with Stokes QU data, to avoid placing excessive weight on Stokes I relative to Stokes VQU data.

4.2. Results for AU Mic and EV Lac

Figure 1 shows the observed LSD Stokes $IVQU$ profiles of both stars, along with the corresponding ZDI fits to the data down to the photon noise level for each of the three imaging cases mentioned above. The best results were obtained for $f_P = 0.2$ and $f_I = 0.9$ for AU Mic, in agreement with Cristofari et al. (2023) and Donati et al. (2023a), and for $f_P = 0.15$ and $f_I = 1.0$ for EV Lac (with a f_I value matching that in Cristofari et al. 2023, 2025). The three ZDI fits to the LSD Stokes V profiles and the two fits to the LSD Stokes I profiles (depicted with different colors in the first- and second-column plots of Fig. 1) are of very similar quality. The derived ZDI images are shown in Fig. 2 for AU Mic, and in Fig. 3 for EV Lac. Reconstructed simultaneously with the magnetic maps, the brightness images show only low-contrast features, as expected from the small amplitude of the photometric curves (see Fig. 4).

For AU Mic, the reconstructed large-scale field is dominantly poloidal in all three reconstructions (see Table 2 where the main magnetic properties of the derived fields are summarized). When considering only the LSD Stokes V profiles (with $v_D = 5.3$ km s^{-1}, see Sect. 4.1), the inferred field is mostly non-axisymmetric, with a global dipole field of only 250 G (see Table 2) and weaker quadrupole and octupole components. The small-scale field derived with ZDI in this initial case (1.6 kG) is significantly weaker than that obtained in the two other imaging cases (4 kG), reflecting that the Zeeman broadening of the LSD Stokes I profiles requires stronger fields when $v_D = 3.5$ km s^{-1}. In our modeling framework, where we assume that the small-scale field grows with the large-scale field (with a scaling factor f_I/f_P), this implies that a significant fraction of the large-scale field is missed when fitting only the LSD Stokes V profiles, as already concluded in Donati et al. (2023a). This effect likely arises from equatorial symmetry in cases like AU Mic, where the rotation axis of the star is nearly perpendicular to the line of sight, causing the Stokes V signatures of odd axisymmetric terms in the SH expansion of the magnetic field to mostly cancel out. The large-scale field that we derive when adjusting both LSD Stokes I and V profiles is almost three times stronger, exceeding 0.9 kG, with a global dipole field of about 1.1 kG and a (mostly aligned) octupole field of about 0.8 kG, storing 70 and 26 percent of the overall magnetic energy reconstructed in the dominant poloidal field component, respectively. These components are stronger in our new reconstruction than in those of our previous paper (Donati et al. 2023a), likely due to both the intrinsic temporal variability and the smearing induced by ZDI when processing Stokes IV data collected over a time span exceeding six months. The two low-latitude, positive radial field features reconstructed in the first imaging case at phases 0.35 and 0.65 now appear only as weak appendages of the main positive radial field feature straddling the pole in the derived Stokes IV image. Including the LSD Stokes QU profiles in the ZDI fit enhances these appendages, but otherwise generates only moderate changes in the reconstructed magnetic topology and its main characteristics (see Table 2). The synthetic QU profiles associated with the Stokes V and Stokes IV reconstructions are often discrepant in amplitude and shape with those of our full Stokes modeling (see Fig. 5, left panels) even though the Stokes IV and Stokes $IVQU$ magnetic maps are not significantly different, emphasizing the importance of collecting Stokes QU data whenever possible. Moreover, this demonstrates that our implementation of ZDI using all LSD Stokes parameters behaves satisfactorily, reliably reproducing LSD Stokes QU profiles with only minor differences from magnetic topologies derived from LSD Stokes IV profiles for stars like AU Mic, whose large-scale field is not overly complex and mostly axisymmetric.

For EV Lac, we also find that the reconstructed large-scale field is largely poloidal in all three cases. The mostly non-axisymmetric large-scale field reconstructed from the LSD Stokes V profiles alone does not properly account for the large Zeeman broadening of the Stokes I profiles, particularly in the far wings. This discrepancy persists even after increasing the scaling factor f_I/f_P between small- and large-scale fields by 50 percent from the AU Mic case, to better match the shape of the strongest observed LSD Stokes V profiles, especially their gradients close to the line center. The reconstructed large-scale field includes a dominant quadrupole term which stores 40 percent of the poloidal field energy and generates 0.6 kG equatorial

Table 2. Properties of the large-scale magnetic field of AU Mic and EV Lac, for the Stokes V, Stokes IV and Stokes $IVQU$ ZDI reconstruction schemes.

Quantity	AU Mic			EV Lac		
	V	IV	$IVQU$	V	IV	$IVQU$
v_D (km s^{-1})	5.3	3.5	3.5	5.3	3.5	3.5
f_P	0.2	0.2	0.2	0.15	0.15	0.15
f_I		0.9	0.9		1.0	1.0
ψ (°)			26 ± 5			86 ± 5
$<B_P>$ (G)	355	935	920	520	995	845
$<B_I>$ (kG)	1.6	4.2	4.1	3.5	6.6	5.6
$<B_{I,max}>$ (kG)	3.5	9.5	10.1	10.3	13.2	12.5
$<B_s>$ (kG)	1.6	2.6	2.6	2.5	4.3	4.2
B_d (kG)	0.25	1.15	1.06	0.34	0.80	0.62
Tilt (°)	34	11	9	90	28	35
Phase	0.54	0.54	0.57	0.92	0.82	0.90
Poloidal (%)	84	98	97	95	89	82
Axisymetry (%)	29	97	96	2	82	54
Pol dipole (%)	37	70	60	32	63	45

Notes. In each case, we list the assumed Doppler width v_D and polarization f_P filling factor used in the ZDI modeling, the inferred values of the angle ψ of the projected stellar rotation axis on the plane of the sky, the reconstructed large-scale field strength $<B_P>$ and corresponding average small-scale field $<B_I>$ quadratically averaged over the whole star, the maximum small-scale field $<B_{I,max}>$ at the surface of the star, the phase-averaged small-scale field $<B_s>$ computed over the visible (limb darkened) stellar hemisphere (directly comparable to the small-scale field $<B>$ measured with ZeeTurbo), the polar strength B_d of the large-scale field dipole component, the tilt of the dipole field to the rotation axis and the phase towards which it is tilted, the amount of magnetic energy reconstructed in the poloidal component of the large-scale field, and in the axisymmetric dipole mode ($m = 0$, $\ell = 1$) of this component. Error bars are typically equal to 10 percent for field strengths and percentages and 5° for field inclinations.

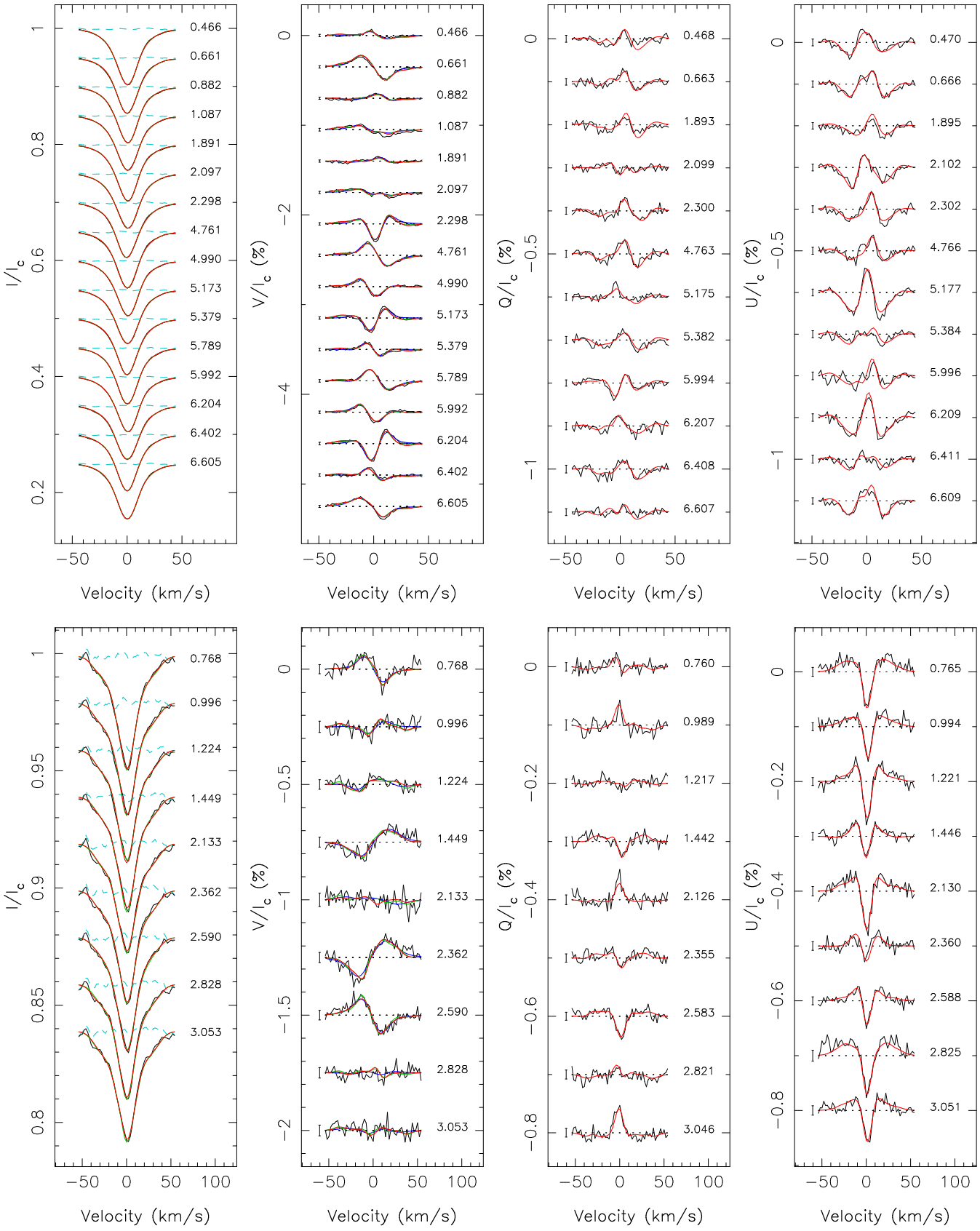

Fig. 1. Observed (thick black line) and modeled (thin color line) LSD Stokes I, V, Q and U profiles (from left to right) of AU Mic (top row) and EV Lac (bottom row). The thin blue, green and red lines correspond, respectively, to the Stokes V, Stokes IV and Stokes $IVQU$ ZDI fits to the LSD profiles; the cyan dashed lines in the left panels illustrate the difference between the observations and the Stokes $IVQU$ ZDI fit. Rotation cycles are indicated to the right of LSD profiles, and $\pm 1\sigma$ error bars are shown to the left of the Stokes VQU signatures.

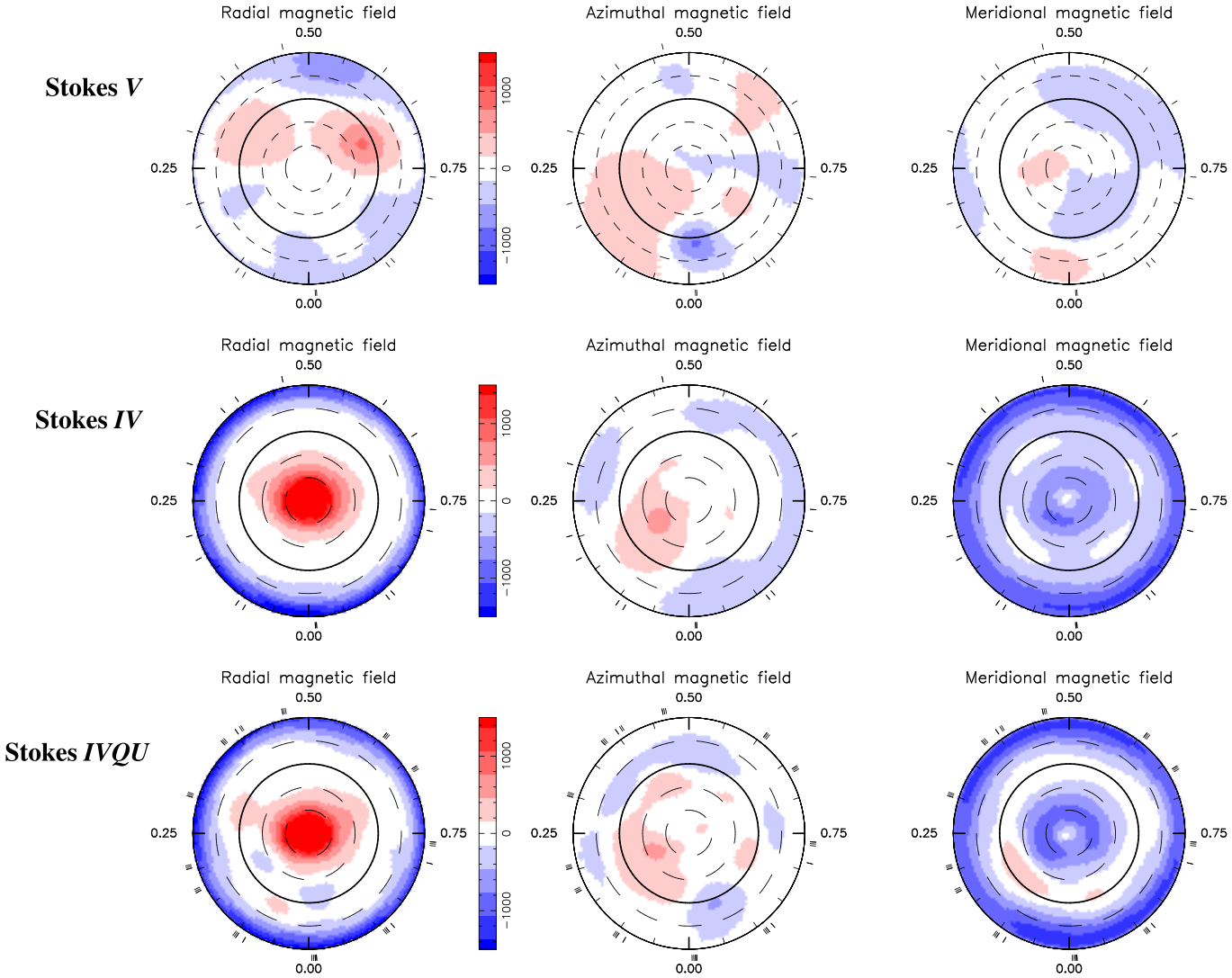

Fig. 2. Reconstructed maps of the large-scale magnetic field of AU Mic using ZDI from Stokes *V* (top row), Stokes *IV* (middle row) and Stokes *IVQU* (bottom row) SPIRou data. In each row, from left to right, the radial, azimuthal and meridional components of the magnetic field in spherical coordinates (in G) are shown. All maps are displayed in a flattened polar projection down to latitude −60°, with the north pole at the center and the equator depicted as a bold line. Outer ticks indicate the phases of the observations. Positive radial, azimuthal and meridional fields point outward, counterclockwise and poleward, respectively.

regions of alternating polarities, a weaker (0.34 kG) highly tilted dipole component, and a weak and complex octupole field. The inferred phase-averaged small-scale field $<B_s>$ computed over the limb-darkened visible stellar hemisphere (2.5 kG) is significantly weaker than that measured with ZeeTurbo. Incorporating the LSD Stokes *I* profiles in the ZDI fit, while reducing $v_{\rm D}$ from 5.3 to 3.5 km s^{-1}, yields a notably different field topology. The radial field component now features a strong positive field region near the pole, accompanied by lower latitude appendages, but still exhibiting a similar polarity pattern with phase (positive radial field at phases 0.1 and 0.6 and negative field at phase 0.4). In this process, both the average large- and small-scale magnetic strengths increase by about 50 percent, reaching approximately 1.0 and 6.6 kG, respectively. The global dipole component also increases to 0.80 kG and becomes dominant. It is no longer orthogonal to the rotation axis but remains significantly tilted (by about 30°). Finally, adding LSD Stokes *QU* profiles to the ZDI fit further complexifies the field. The main field characteristics now show that the dipole field decreases to 0.62 kG but remains dominant (see Table 2). Some power is now present in the higher SH modes; for example, a negative radial field region now appears at low latitudes near phase 0.0. More than for AU Mic, the synthetic *QU* profiles associated with the Stokes *V* and Stokes *IV* reconstructions are often grossly inconsistent in both amplitude and shape compared to those from our full Stokes modeling (see Fig. 5, right panels). This emphasizes again that LSD Stokes *QU* profiles can provide key information about the large-scale and small-scale magnetic topologies, especially for low-$v \sin i$ stars such as EV Lac, whose narrow spectral lines contain limited spatial information about stellar surface features.

We caution that, although our ZDI reconstruction of EV Lac is made unique by construction (i.e., by choosing the simplest solution consistent with the data for the selected parameters, see Sect. 4.1), the inversion problem is still degenerate to some extent in cases where the rotational broadening, the spectral resolution, the number of observed profiles, and the S/N are limited, even when all Stokes profiles are included in the process. We suspect that different, even more complex magnetic topologies, may also exist for EV Lac, matching equally well the LSD

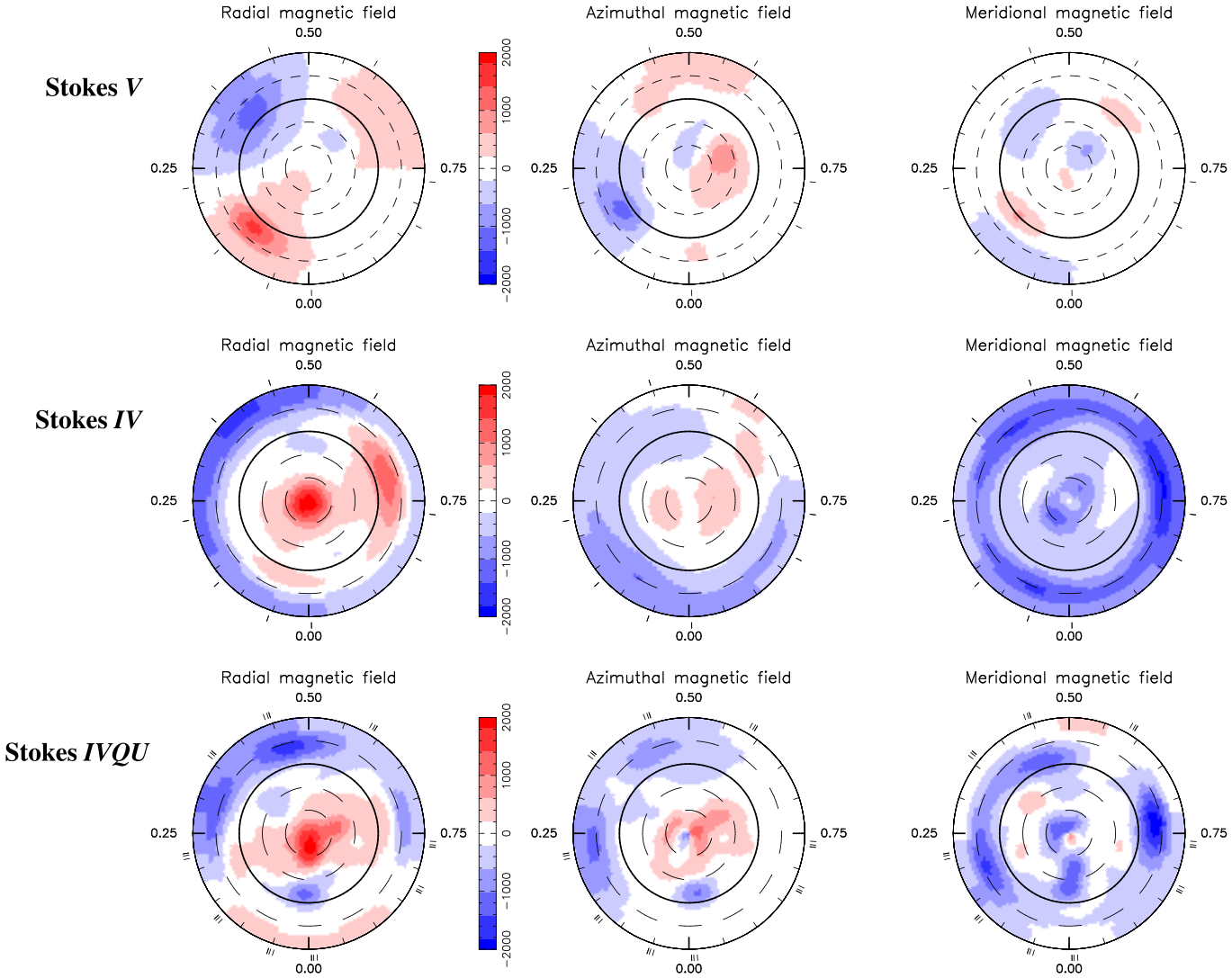

Fig. 3. Same as Fig. 2 for EV Lac.

Stokes $IVQU$ data. The situation is more favorable for AU Mic where the higher $v \sin i$ stabilizes the inversion and yields a more constrained solution.

To further assess the consistency of our ZDI reconstructions from all Stokes profiles, we computed for both stars the small-scale fields that we expect from the derived magnetic topologies, as if measured from the spectra over the visible stellar hemispheres, as well as their rotational modulation (see Fig. 6). In both cases, we find small-scale field values and modulation that are reasonably consistent with ZeeTurbo measurements, in the range 2.4–2.9 kG for AU Mic and 3.7–4.4 kG for EV Lac (see Tables A.1 and A.2 and Cristofari et al. 2023; Donati et al. 2023a; Cristofari et al. 2025), even though the modulation amplitude we recover with ZDI for EV Lac is smaller than what ZeeTurbo indicates (missing the dip at phase 0.4). This confirms, in particular, that reconstructions from LSD Stokes IV and $IVQU$ profiles yield a much better match to observations than those from LSD Stokes V profiles alone.

We also derived potential field extrapolations of the large-scale field of both stars as seen from an Earth-based observer, using the radial field maps derived from all LSD Stokes profiles (see Fig. 7) and assuming a source surface located at 5 $R_\star$.

5. Discussion and conclusions

In this paper, we present a spectropolarimetric analysis of the well-known active M dwarfs AU Mic and EV Lac, based on a set of 67 circularly and linearly polarized spectra collected on both stars with SPIRou at CFHT from August to October 2023, covering a few rotational cycles. We first used LSD to derive the Zeeman signatures associated with these spectra from about 1500 atomic lines. We detected the weak LSD Stokes QU signals of both stars at most observed phases in addition to the much stronger Stokes IV signals usually recorded on M dwarfs with SPIRou. We then employed ZDI to reconstruct the magnetic topologies at the surface of both stars, using either LSD Stokes V data alone, LSD Stokes IV profiles, or the full set of LSD Stokes $IVQU$ observations. This approach allowed us to investigate in detail how the inferred topologies differ and what additional information each type of data brings to the inversion problem, helping to reduce potential degeneracies. In the second and third cases, we further constrained ZDI by simultaneously reconstructing surface brightness distributions, fitting photometric light curves derived from dT measurements at the same time as LSD Stokes profiles.

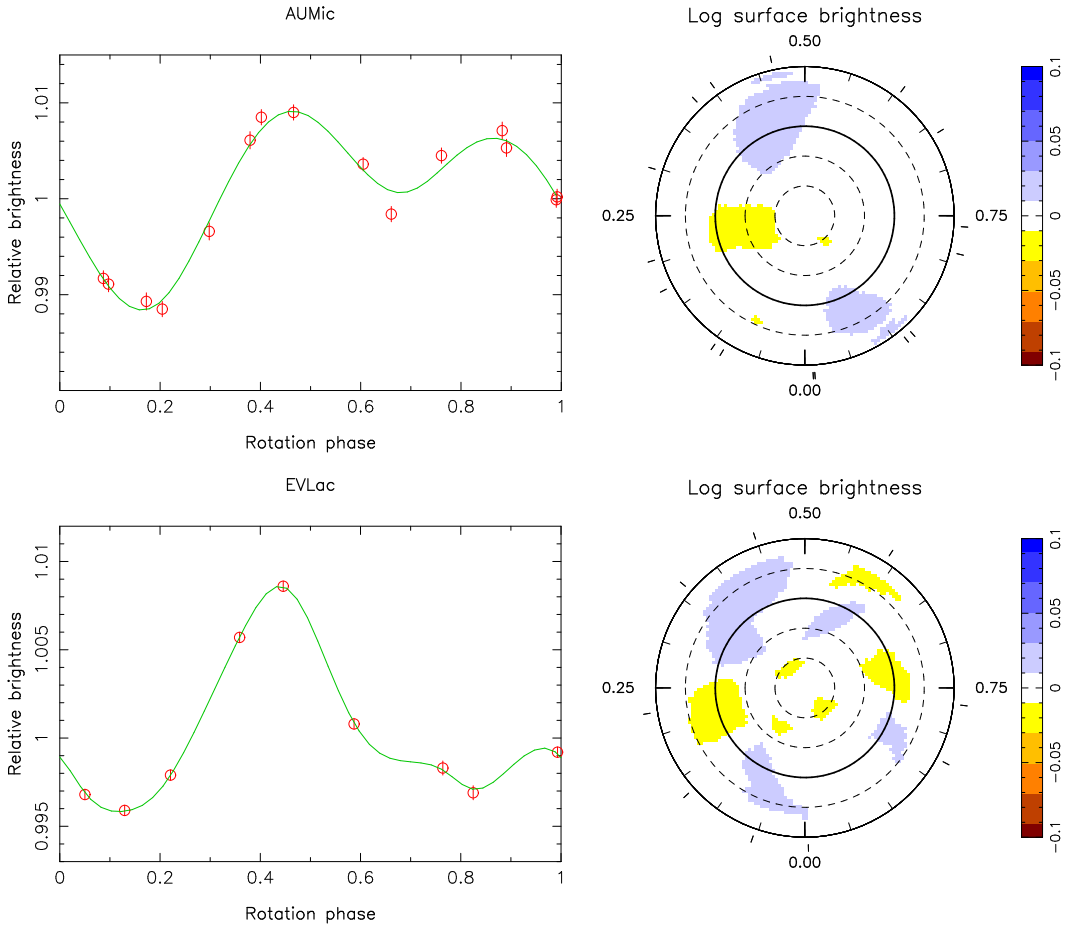

Fig. 4. Photometric light curves inferred from dT estimates (red circles, left panels) with ZDI fits (green curves), and brightness maps (right panels) reconstructed simultaneously with the magnetic maps of Figs. 2 and 3, for both AU Mic (top row) and EV Lac (bottom row), in the case of Stokes $IVQU$ reconstructions. Very similar results are obtained in Stokes IV reconstructions. The brightness maps are shown as in Figs. 2 and 3, with yellow and blue depicting regions darker and brighter than the quiet photosphere, respectively.

The magnetic imaging process and ZDI routines used in this study are the same as in Donati et al. (2023a), which we have now also applied to datasets including LSD Stokes QU profiles. When running ZDI on LSD Stokes V profiles only (and setting $v_{\rm D}$ = 5.3 km s^{-1} to match the average width of LSD Stokes I profiles, as in Donati et al. 2023a), the inferred large-scale magnetic topology of both stars is mostly non-axisymmetric, and the quadratically averaged large-scale and small-scale fields over the stellar surfaces reach only 355 G and 1.6 kG for AU Mic, and 520 G and 3.5 kG for EV Lac. When adjusting LSD Stokes I and V profiles simultaneously (setting now $v_{\rm D}$ = 3.5 km s^{-1}), the large-scale and small-scale fields both increase to about 935 G and 4.2 kG for AU Mic, and 1.0 kG and 6.6 kG for EV Lac. The large-scale field is now dominantly axisymmetric and incorporates a stronger dipole component, of about 1.1 kG and 0.8 kG in the case of AU Mic and EV Lac, respectively. When fitting all LSD Stokes profiles at once, the large-scale and small-scale fields evolve again, though less so for AU Mic than for EV Lac. Our results also show that our simple parametric approach to describe both the large-scale and small-scale fields at the surface of the star within ZDI is successful at reproducing observations in a consistent way. However, we caution that, given the low $v \sin i$ and the limited S/N and spatial information enclosed in spectral lines, the inversion problem is still ill-posed, particularly for EV Lac, even for reconstructions from Stokes $IVQU$ data. More complex solutions may still exist, matching all LSD profiles equally well.

The magnetic topology we recover for AU Mic from all Stokes profiles is fairly simple, with almost all of the recovered magnetic energy stored in the dipole and octupole field components. Both are mostly aligned with the rotation axis and thus perpendicular to the line of sight. We do not expect the nearly equator-on orientation of AU Mic to be the main cause of the reconstructed largely axisymmetric magnetic topology, especially when all Stokes profiles are fitted. The larger $v \sin i$ indeed allows non-axisymmetric structures to be more reliably recovered. The large-scale magnetic topology of AU Mic is conveniently oriented for Earth-based observers to detect and monitor radio emission, particularly the reported highly circularly polarized and rotationally modulated bursts of coherent beamed emission generated by the electron cyclotron maser instability that are likely taking place in the auroral rings of the magnetic poles (Bloot et al. 2024). Given the stronger large-scale dipole field derived in our new study, one can expect a wider Alfven volume than that initially estimated (Kavanagh et al. 2021; Alvarado-Gómez et al. 2022). This implies that the two transiting planets (b and c) are likely located within this volume and thus able to magnetically interact with their host star. However, the observed radio bursts from AU Mic have not shown periodicity at the orbital or the synodic periods of the planets during the radio monitoring campaign of Bloot et al. (2024). This suggests that the transiting planets do not induce beamed radio emission as a result of star-planet interactions, or that the corresponding radio flux is weaker than expected. It nonetheless

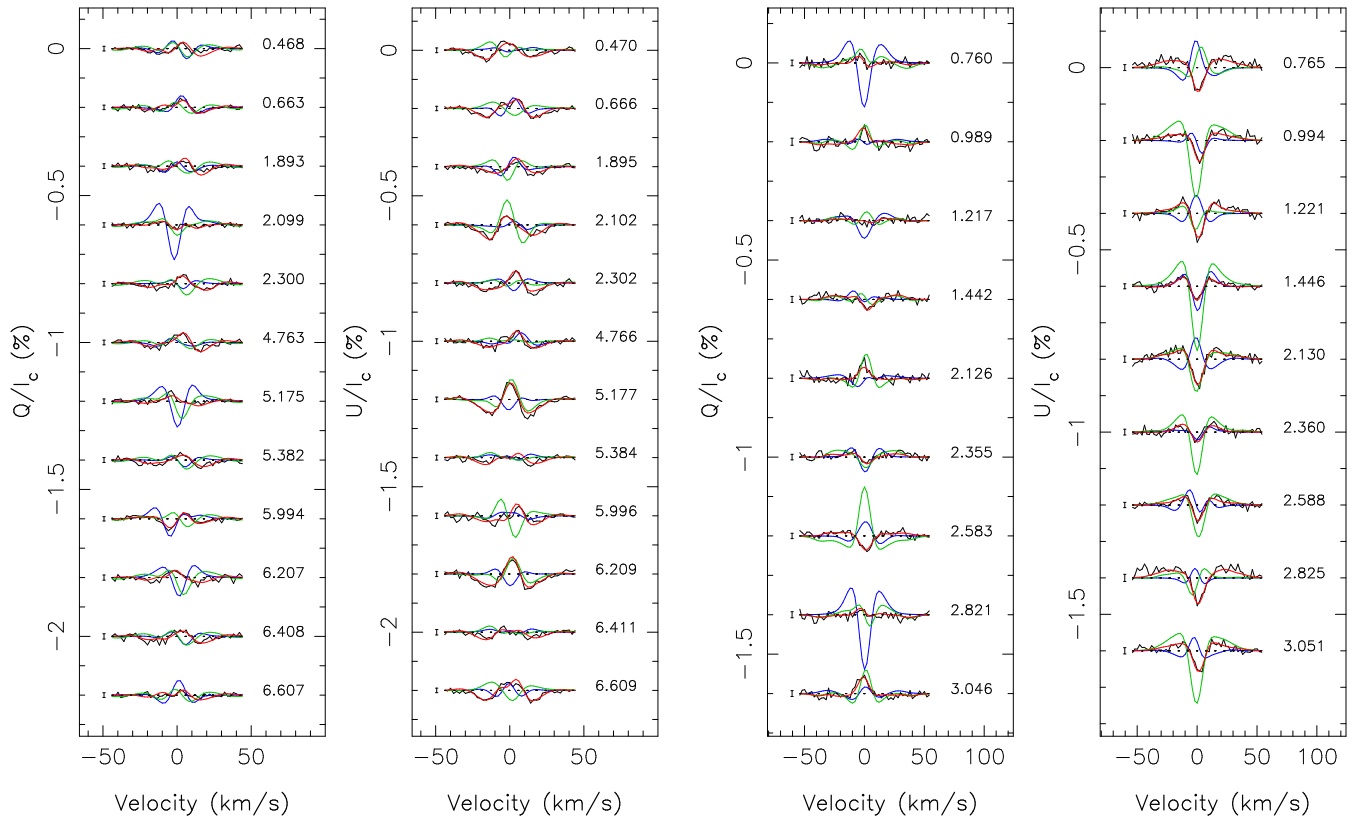

Fig. 5. Same as the two rightmost panels of Fig. 1, now also showing the synthetic Stokes *QU* profiles associated with the Stokes *V* (blue line) and *IV* (green line) reconstructions, for both AU Mic (left panels) and EV Lac (right panels).

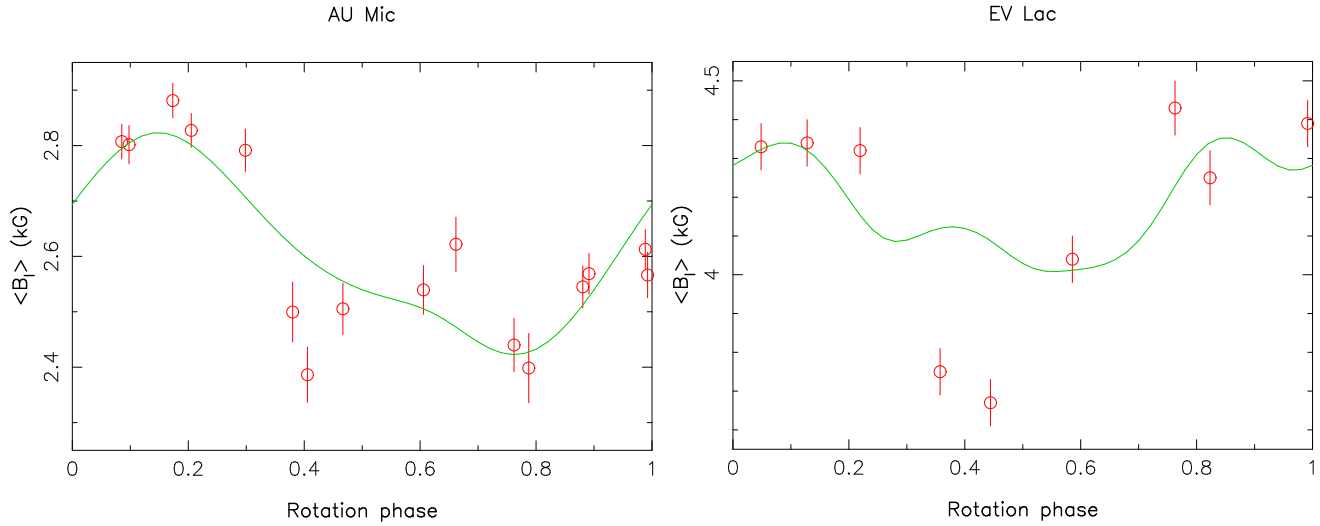

Fig. 6. Rotational modulation of the small-scale field $<B_l>$ (green curve), computed over the visible limb-darkened stellar hemisphere and derived from our ZDI reconstructions of AU Mic (left panel) and EV Lac (right panel), compared to the actual average small-scale field $<B_s>$ directly measured from individual Stokes *I* spectra with ZeeTurbo (red circles, Cristofari et al. 2023, 2025).

sets AU Mic as an ideal laboratory for studying radio emission from the electron cyclotron maser instability, whether caused by activity or induced by close-in planets, for objects other than the Sun and Jupiter.

The magnetic topology we infer for EV Lac from all Stokes profiles is stronger, more complex, and more tilted with respect to the rotation axis than that of AU Mic. It has a weaker (though still dominant) dipole component and significant power in higher terms of the SH expansion, inducing smaller magnetic features at the stellar surface. Our results show, in particular, that the large-scale field of EV Lac and its dipole component are not highly tilted to the rotation axis, as initially suggested from magnetic maps reconstructed from Stokes *V* data only (Morin et al. 2008; Bellotti et al. 2024). Despite their residual non-axisymmetry, our new magnetic maps of EV Lac are much more consistent with the magnetic topologies of other M dwarfs with similar internal structure (such as AU Mic or AD Leo). The more complex magnetic geometry of EV Lac, compared to that of AU Mic, may

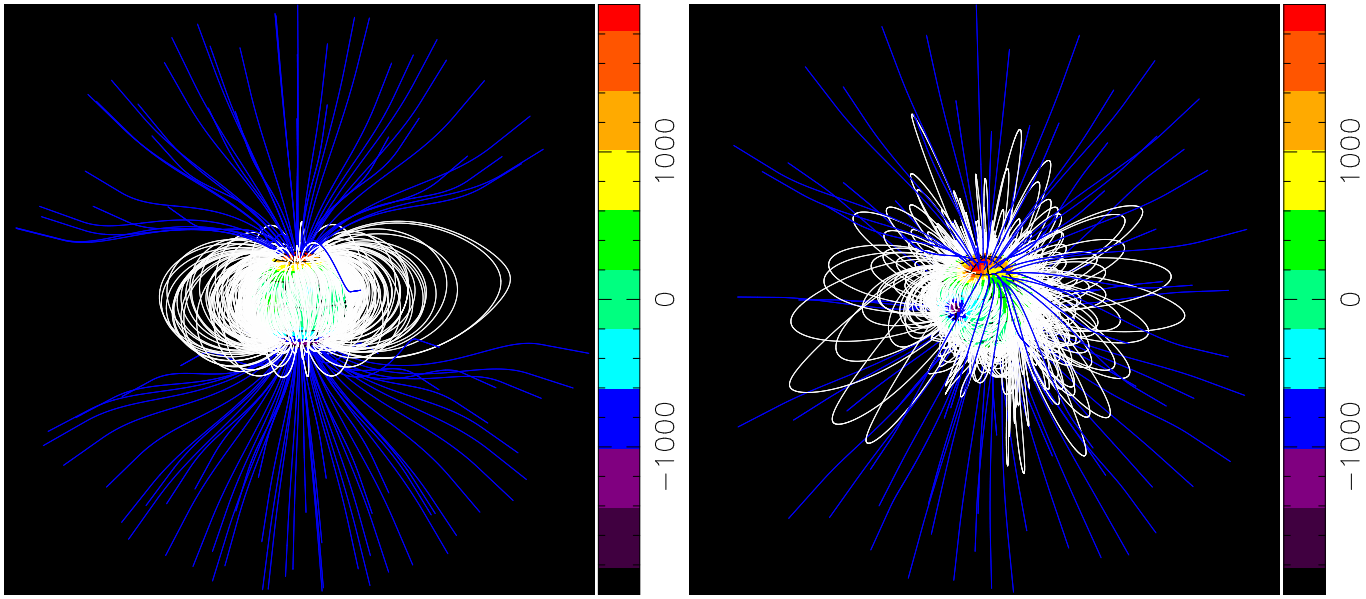

Fig. 7. Potential field extrapolation of the large-scale field topologies derived with ZDI from our SPIRou Stokes $IVQU$ observations of AU Mic (left panel) and EV Lac (right panel). Open field lines are shown in blue and closed field lines in white. The color scale indicates the value of the radial field at the surface of the star (in G), as derived by ZDI. The stars are shown as viewed from the Earth at rotational phases 0.20 and 0.90, respectively, with the source surface arbitrarily set to 5 $R_\star$. Animated movies are available online.

explain why EV Lac exhibits one of the highest fractions of flaring time among a sample of active M dwarfs (including AU Mic, Paudel et al. 2024). The more complex the magnetic topology, the smaller the size of closed field loops at the surface of the star, and the more frequent flaring is likely to happen as a result of reconnection triggered by surface convection and differential rotation. More reconstructions of magnetic topologies of M dwarfs, derived from rotationally modulated sets of LSD Stokes $IVQU$ (or at least Stokes IV) profiles, are needed to further document how magnetic complexity depends on stellar parameters. At the same time, further dynamo simulations are required to explore these aspects in more depth.

Our results suggest that magnetometric studies of active stars with kG fields, including T Tauri stars, benefit from spectropolarimetric observations with SPIRou carried out in all Stokes parameters, provided the required S/N can be reached for Stokes QU Zeeman signatures to be detected. This allows their magnetic topologies to be reconstructed more reliably, especially for stars with medium $v \sin i$'s for which the Zeeman distortions of spectral lines are not drowned out by rotational broadening. Further improvement should also come from gaining simultaneous spectropolarimetric access to both optical and nIR domains. This would allow spectral line distortions from magnetic fields to be disentangled from those induced by brightness features, and both could be consistently reconstructed with ZDI from sets of rotationally modulated line profiles (as in Donati et al. 2024). This will become possible at CFHT once VISION, the forthcoming interface allowing both ESPaDOnS and SPIRou to operate simultaneously with no loss of polarimetric efficiency, is implemented at the telescope, which is expected to occur in the second semester of 2026.

Data availability

SPIRou data used in this study are publicly available from the Canadian Astronomy Data Center (https://www.cadc-ccda.hia-iha.nrc-cnrc.gc.ca), except for the SPICE data that will be available from 2025 September 01.
Movies associated to Fig. 7 are available at https://www.aanda.org

Acknowledgements. This work benefited from the SIMBAD CDS database at URL http://simbad.u-strasbg.fr/simbad and the ADS system at URL https://ui.adsabs.harvard.edu. Our study is based on data obtained at the CFHT, operated by the CNRC (Canada), INSU/CNRS (France) and the University of Hawaii. The authors wish to recognise and acknowledge the very significant cultural role and reverence that the summit of Maunakea has always had within the indigenous Hawaiian community.

References

Alvarado-Gómez, J. D., Cohen, O., Drake, J. J., et al. 2022, ApJ, 928, 147
Artigau, É., Malo, L., Doyon, R., et al. 2018, AJ, 155, 198
Artigau, É., Cadieux, C., Cook, N. J., et al. 2022, AJ, 164, 84
Artigau, É., Cadieux, C., Cook, N. J., et al. 2024, AJ, 168, 252
Baraffe, I., Homeier, D., Allard, F., & Chabrier, G. 2015, A&A, 577, A42
Bellotti, S., Morin, J., Lehmann, L. T., et al. 2024, A&A, 686, A66
Bloot, S., Callingham, J. R., Vedantham, H. K., et al. 2024, A&A, 682, A170
Boccaletti, A., Thalmann, C., Lagrange, A.-M., et al. 2015, Nature, 526, 230
Boccaletti, A., Sezestre, E., Lagrange, A. M., et al. 2018, A&A, 614, A52
Boldog, Á., Szabó, G. M., Kriskovics, L., et al. 2025, A&A, 694, A137
Boro Saikia, S., Lueftinger, T., Jeffers, S. V., et al. 2018, A&A, 620, L11
Cale, B. L., Reefe, M., Plavchan, P., et al. 2021, AJ, 162, 295
Cook, N. J., Artigau, É., Doyon, R., et al. 2022, PASP, 134, 114509
Cristofari, P. I., Donati, J. F., Masseron, T., et al. 2022, MNRAS, 511, 1893
Cristofari, P. I., Donati, J. F., Folsom, C. P., et al. 2023, MNRAS, 522, 1342
Cristofari, P. I., Donati, J.-F., Belloti, S., et al. 2025, A&A, Submitted
Donati, J., & Landstreet, J. D. 2009, ARA&A, 47, 333
Donati, J.-F., Brown, S. F., Semel, M., et al. 1992a, A&A, 265, 682
Donati, J. F., Semel, M., & Rees, D. E. 1992b, A&A, 265, 669
Donati, J.-F., Semel, M., Carter, B. D., Rees, D. E., & Collier Cameron, A. 1997, MNRAS, 291, 658
Donati, J.-F., Howarth, I. D., Jardine, M. M., et al. 2006, MNRAS, 370, 629
Donati, J. F., Kouach, D., Moutou, C., et al. 2020, MNRAS, 498, 5684
Donati, J. F., Cristofari, P. I., Finociety, B., et al. 2023a, MNRAS, 525, 455
Donati, J. F., Lehmann, L. T., Cristofari, P. I., et al. 2023b, MNRAS, 525, 2015
Donati, J. F., Finociety, B., Cristofari, P. I., et al. 2024, MNRAS, 530, 264
Donati, J.-F., Cristofari, P. I., Moutou, C., et al. 2025, A&A, in press https://doi.org/10.1051/0004-6361/202555371

Engle, S. G. 2024, ApJ, 960, 62
Fares, R., Donati, J. F., Moutou, C., et al. 2009, MNRAS, 398, 1383
Favata, F., Reale, F., Micela, G., et al. 2000, A&A, 353, 987
Feiden, G. A. 2016, A&A, 593, A99
Feinstein, A. D., France, K., Youngblood, A., et al. 2022, AJ, 164, 110
Finociety, B., & Donati, J. F. 2022, MNRAS, 516, 5887
Fouqué, P., Martioli, E., Donati, J. F., et al. 2023, A&A, 672, A52
Gaia Collaboration (Brown, A. G. A., et al.) 2021, A&A, 649, A1
Gallenne, A., Desgrange, C., Milli, J., et al. 2022, A&A, 665, A41
Hébrard, É. M., Donati, J. F., Delfosse, X., et al. 2016, MNRAS, 461, 1465
Ibañez Bustos, R. V., Buccino, A. P., Flores, M., et al. 2019, MNRAS, 483, 1159
Johns-Krull, C. M., & Valenti, J. A. 1996, ApJ, 459, L95
Kavanagh, R. D., Vidotto, A. A., Klein, B., et al. 2021, MNRAS, 504, 1511
Klein, B., Donati, J.-F., Moutou, C., et al. 2021, MNRAS, 502, 188
Klein, B., Zicher, N., Kavanagh, R. D., et al. 2022, MNRAS, 512, 5067
Kochukhov, O. 2021, A&A Rev., 29, 1
Kochukhov, O., & Reiners, A. 2020, ApJ, 902, 43
Kochukhov, O., Bagnulo, S., Wade, G. A., et al. 2004, A&A, 414, 613
Kochukhov, O., Hackman, T., & Lehtinen, J. J. 2023, A&A, 680, L17
Landi degl'Innocenti, E., & Landolfi, M. 2004, Polarisation in Spectral Lines (Dordrecht/Boston/London: Kluwer Academic Publishers)
Lawson, K., Schlieder, J. E., Leisenring, J. M., et al. 2023, AJ, 166, 150
Lehmann, L. T., & Donati, J. F. 2022, MNRAS, 514, 2333
Lehmann, L. T., Donati, J. F., Fouqué, P., et al. 2024, MNRAS, 527, 4330
Mallorquín, M., Béjar, V. J. S., Lodieu, N., et al. 2024, A&A, 689, A132
Martioli, E., Hébrard, G., Correia, A. C. M., Laskar, J., & Lecavelier des Etangs, A. 2021, A&A, 649, A177
Morin, J., Donati, J.-F., Petit, P., et al. 2008, MNRAS, 390, 567
Morin, J., Donati, J., Petit, P., et al. 2010, MNRAS, 407, 2269
Paudel, R. R., Barclay, T., Youngblood, A., et al. 2024, ApJ, 971, 24
Piskunov, N. 2005, in EAS Publications Series, 17, eds. G. Alecian, O. Richard, & S. Vauclair, 245
Plavchan, P., Barclay, T., Gagné, J., et al. 2020, Nature, 582, 497
Reiners, A. 2012, Liv. Rev. Sol. Phys., 9, 1
Reiners, A., & Basri, G. 2007, ApJ, 656, 1121
Reiners, A., Shulyak, D., Käpylä, P. J., et al. 2022, A&A, 662, A41
Rescigno, F., Mortier, A., Dumusque, X., et al. 2024, MNRAS, 532, 2741
Robinson, R. D., Worden, S. P., & Harvey, J. W. 1980, ApJ, 236, L155
Rosén, L., Kochukhov, O., & Wade, G. A. 2015, ApJ, 805, 169
Ryabchikova, T., Piskunov, N., Kurucz, R. L., et al. 2015, Phys. Scr, 90, 054005
Saar, S. H., & Linsky, J. L. 1985, ApJ, 299, L47
See, V., Jardine, M., Vidotto, A. A., et al. 2015, MNRAS, 453, 4301
Skilling, J., & Bryan, R. K. 1984, MNRAS, 211, 111
Strugarek, A., Brun, A. S., Matt, S. P., & Réville, V. 2015, ApJ, 815, 111
Szabó, G. M., Garai, Z., Brandeker, A., et al. 2022, A&A, 659, L7
Vidotto, A. A., Jardine, M., Morin, J., et al. 2013, A&A, 557, A67
Vidotto, A. A., Gregory, S. G., Jardine, M., et al. 2014, MNRAS, 441, 2361
Waalkes, W. C., Berta-Thompson, Z. K., Newton, E. R., et al. 2024, ApJ, 962, 97
Wittrock, J. M., Plavchan, P. P., Cale, B. L., et al. 2023, AJ, 166, 232
Wright, N. J., Newton, E. R., Williams, P. K. G., Drake, J. J., & Yadav, R. K. 2018, MNRAS, 479, 2351
Yadav, R. K., Christensen, U. R., Morin, J., et al. 2015, ApJ, 813, L31
Yu, H., Garai, Z., Cretignier, M., et al. 2025, MNRAS, 536, 2046
Zicher, N., Barragán, O., Klein, B., et al. 2022, MNRAS, 512, 3060

Appendix A: Observation log

Tables A.1 and A.2 gives the full log of Stokes VQU spectropolarimetric SPIRou observations of AU Mic and EV Lac from August to October 2023.

Table A.1: Observing log of our Stokes VQU spectropolarimetric SPIRou observations of AU Mic in August 2023

BJD (2459000+)	UT date	Star	c / ϕ	t_{exp} (s)	S/N (H)	σ_P ($10^{-4} I_c$)	Stokes	B_ℓ (G)	$<B_s>$ (kG)	dT (K)
1158.9450165	02 Aug 2023	AU Mic	238 / 0.466	802.4	834	0.81	V	5±4	2.51±0.05	19.19±1.18
1158.9557904	02 Aug 2023	AU Mic	238 / 0.468	802.4	845	0.63	Q			
1158.9664817	02 Aug 2023	AU Mic	238 / 0.470	802.4	845	0.64	U			
1159.8927438	03 Aug 2023	AU Mic	238 / 0.661	802.4	889	0.80	V	93±4	2.62±0.05	3.70±1.14
1159.9035273	03 Aug 2023	AU Mic	238 / 0.663	802.4	876	0.61	Q			
1159.9143589	03 Aug 2023	AU Mic	238 / 0.666	802.4	895	0.61	U			
1160.9676210	04 Aug 2023	AU Mic	238 / 0.882	802.4	920	0.74	V	-13±4	2.54±0.04	16.45±1.31
1161.9622558	05 Aug 2023	AU Mic	239 / 0.087	802.4	893	0.95	V	76±5	2.81±0.03	-6.09±1.21
1165.8684823	09 Aug 2023	AU Mic	239 / 0.891	802.4	908	0.80	V	-12±4	2.57±0.04	13.82±1.26
1165.8795421	09 Aug 2023	AU Mic	239 / 0.893	802.4	925	0.64	Q			
1165.8903909	09 Aug 2023	AU Mic	239 / 0.895	802.4	923	0.61	U			
1166.8725352	10 Aug 2023	AU Mic	240 / 0.097	802.4	882	0.77	V	62±4	2.80±0.03	-6.97±1.21
1166.8834741	10 Aug 2023	AU Mic	240 / 0.099	802.4	850	0.59	Q			
1166.8938495	10 Aug 2023	AU Mic	240 / 0.102	802.4	772	0.65	U			
1167.8481084	11 Aug 2023	AU Mic	240 / 0.298	802.4	904	0.84	V	11±4	2.79±0.04	1.06±1.25
1167.8590500	11 Aug 2023	AU Mic	240 / 0.300	802.4	907	0.63	Q			
1167.8697311	11 Aug 2023	AU Mic	240 / 0.302	802.4	905	0.64	U			
1179.8186449	23 Aug 2023	AU Mic	242 / 0.761	802.4	844	0.86	V	79±4	2.44±0.05	12.64±1.16
1179.8302123	23 Aug 2023	AU Mic	242 / 0.763	802.4	860	0.63	Q			
1179.8420478	23 Aug 2023	AU Mic	242 / 0.766	802.4	880	0.66	U			
1180.9308369	24 Aug 2023	AU Mic	242 / 0.990	802.4	867	0.92	V	17±4	2.61±0.04	5.83±1.13
1181.8186111	25 Aug 2023	AU Mic	243 / 0.173	802.4	866	0.84	V	-16±4	2.88±0.03	-9.74±1.31
1181.8298154	25 Aug 2023	AU Mic	243 / 0.175	802.4	851	0.63	Q			
1181.8406102	25 Aug 2023	AU Mic	243 / 0.177	802.4	837	0.65	U			
1182.8234064	26 Aug 2023	AU Mic	243 / 0.379	802.4	830	0.94	V	27±5	2.50±0.05	15.01±1.31
1182.8342156	26 Aug 2023	AU Mic	243 / 0.382	802.4	832	0.66	Q			
1182.8451345	26 Aug 2023	AU Mic	243 / 0.384	802.4	831	0.66	U			
1184.8133935	28 Aug 2023	AU Mic	243 / 0.789	802.4	894	0.90	V	71±4	2.40±0.06	
1185.7993039	29 Aug 2023	AU Mic	243 / 0.992	802.4	902	0.82	V	14±4	2.57±0.04	6.39±1.23
1185.8100395	29 Aug 2023	AU Mic	243 / 0.994	802.4	908	0.58	Q			
1185.8207370	29 Aug 2023	AU Mic	243 / 0.996	802.4	891	0.73	U			
1186.8327092	30 Aug 2023	AU Mic	244 / 0.204	802.4	740	0.91	V	-20±4	2.83±0.03	-10.81±1.19
1186.8438843	30 Aug 2023	AU Mic	244 / 0.207	802.4	717	0.70	Q			
1186.8546516	30 Aug 2023	AU Mic	244 / 0.209	802.4	709	0.71	U			
1187.7936592	31 Aug 2023	AU Mic	244 / 0.402	802.4	670	0.95	V	16±5		18.52±1.16
1187.8247707	31 Aug 2023	AU Mic	244 / 0.408	802.4	691	0.71	Q			
1187.8355074	31 Aug 2023	AU Mic	244 / 0.411	802.4	650	0.74	U			
1188.7797490	01 Sep 2023	AU Mic	244 / 0.605	802.4	870	0.77	V	92±4	2.54±0.04	11.29±1.07
1188.7903324	01 Sep 2023	AU Mic	244 / 0.607	802.4	882	0.64	Q			
1188.8013085	01 Sep 2023	AU Mic	244 / 0.609	802.4	896	0.61	U			

Notes. All exposures consist of 4 sub-exposures of equal length. For each star and each visit, we list the barycentric Julian date BJD, the UT date, the rotation cycle c and phase ϕ (computed as indicated in Sect. 3), the total observing time t_{exp}, the peak S/N in the spectrum (in the H band) per 2.3 km s^{-1} pixel, the noise level in the LSD Stokes profile, the estimated B_ℓ with error bars (for Stokes V profiles only), the measured small-scale field $<B_s>$ and differential temperature dT with error bars (for each observing night).

Table A.2: Same as Table A.1 for our Stokes VQU spectropolarimetric SPIRou observations of EV Lac in September and October 2023

BJD (2459000+)	UT date	Star	c / ϕ	t_{exp} (s)	S/N (H)	σ_P ($10^{-4} I_c$)	Stokes	B_ℓ (G)	$<B_s>$ (kG)	dT (K)
1213.8123356	26 Sep 2023	EV Lac	277 / 0.760	1582.4	902	0.65	Q			
1213.8321239	26 Sep 2023	EV Lac	277 / 0.765	1582.4	901	0.74	U			
1213.8441117	26 Sep 2023	EV Lac	277 / 0.768	245.2	360	1.88	V	10±25	4.43±0.07	1.81±0.12
1214.8121319	27 Sep 2023	EV Lac	277 / 0.989	1582.4	813	0.82	Q			
1214.8321833	27 Sep 2023	EV Lac	277 / 0.994	1582.4	776	0.66	U			
1214.8443879	27 Sep 2023	EV Lac	277 / 0.996	245.2	291	2.24	V	-105±30	4.39±0.06	2.94±0.09
1215.8081612	28 Sep 2023	EV Lac	278 / 0.217	1582.4	837	0.66	Q			
1215.8278955	28 Sep 2023	EV Lac	278 / 0.221	1582.4	837	0.66	U			
1215.8398404	28 Sep 2023	EV Lac	278 / 0.224	245.2	346	1.93	V	42±25	4.32±0.06	1.29±0.09
1216.7910424	29 Sep 2023	EV Lac	278 / 0.442	1582.4	880	0.70	Q			
1216.8108550	29 Sep 2023	EV Lac	278 / 0.446	1582.4	869	0.63	U			
1216.8228885	29 Sep 2023	EV Lac	278 / 0.449	245.2	349	1.98	V	-228±27	3.67±0.06	14.58±0.10
1219.7787074	02 Oct 2023	EV Lac	279 / 0.126	1582.4	698	0.75	Q			
1219.7986450	02 Oct 2023	EV Lac	279 / 0.130	1582.4	686	0.78	U			
1219.8103943	02 Oct 2023	EV Lac	279 / 0.133	245.2	266	2.53	V	132±37	4.34±0.06	-1.21±0.09
1220.7811537	03 Oct 2023	EV Lac	279 / 0.355	1582.4	801	0.65	Q			
1220.8010876	03 Oct 2023	EV Lac	279 / 0.360	1582.4	752	0.71	U			
1220.8127874	03 Oct 2023	EV Lac	279 / 0.362	245.2	333	1.99	V	-256±28	3.75±0.06	10.95±0.09
1221.7787608	04 Oct 2023	EV Lac	279 / 0.583	1582.4	846	0.62	Q			
1221.7982896	04 Oct 2023	EV Lac	279 / 0.588	1582.4	858	0.66	U			
1221.8104245	04 Oct 2023	EV Lac	279 / 0.590	245.2	346	1.88	V	166±25	4.04±0.06	4.93±0.08
1222.8161946	05 Oct 2023	EV Lac	279 / 0.821	1582.4	891	0.70	Q			
1222.8363693	05 Oct 2023	EV Lac	279 / 0.825	1582.4	895	0.90	U			
1222.8485126	05 Oct 2023	EV Lac	279 / 0.828	245.2	358	2.00	V	-33±30	4.25±0.07	0.14±0.11
1223.8012741	06 Oct 2023	EV Lac	280 / 0.046	1582.4	825	0.67	Q			
1223.8211277	06 Oct 2023	EV Lac	280 / 0.051	1582.4	786	0.78	U			
1223.8332969	06 Oct 2023	EV Lac	280 / 0.053	245.2	326	2.07	V	49±30	4.33±0.06	-0.05±0.09

Notes. Longer exposure times were used for Stokes QU observations to ensure detection of the Zeeman signatures.